Research Square

Preprints are preliminary reports that have not undergone peer review.
They should not be considered conclusive, used to inform clinical practice,
or referenced by the media as validated information.

EphrinB2 Upregulation in Cancer-associated Fibroblasts supports Breast Cancer Stem Cell Niche Formation and Self-Renewal

Paula Dorsch
University Hospital RWTH Aachen
Axel Ihl
University Hospital RWTH Aachen
Lena Hahnfeld
University Hospital RWTH Aachen
Thomas Hansen
University Hospital RWTH Aachen
Anja-Solveig Steinle
University Hospital RWTH Aachen
Roman David Bülow
Universitätsklinikum Aachen
Harshini Muralidharan
University Hospital RWTH Aachen
Elmar Stickeler
University Hospital RWTH Aachen
Jochen Maurer
jmaurer@ukaachen.de

University Hospital RWTH Aachen

Research Article

Keywords: Cancer-associated fibroblasts, Cancer stem cells, Breast Cancer, Tumor Microenvironment, Triple-negative Breast Cancer, EphrinB2, Encapsulation, Self-Renewal, Stemness

Posted Date: November 18th, 2026

DOI: https://doi.org/10.21203/rs.3.rs-11453670/v1

License: This work is licensed under a Creative Commons Attribution 4.0 International License.
Read Full License

Additional Declarations: No competing interests reported.

Abstract

Background

Breast cancer is the most common cancer in women. Triple-negative breast cancer (TNBC) is the most aggressive subtype associated with poor survival and few targeted therapy options. Breast cancer stem cells (BCSCs) are a subpopulation of cancer cells characterized by self-renewal, dormancy, proliferation, differentiation potential and are associated with metastasis, recurrence and resistance. The tumor microenvironment (TME) was found to provide a tumor-supporting niche for these BCSCs, with are cancer-associated fibroblasts (CAFs) as one of the main components. In this work we wanted to investigate mechanisms of interaction between BCSCs and stroma, the consequent induction of CAFs and their cancer-promoting characteristics. We focused on the role of EphrinB2 in the generation of CAFs, as its expression is upregulated in fibroblasts upon contact with BCSCs.

Methods

To investigate a loss-of-function phenotype for EphrinB2, we created a lentiviral knockdown (KD) of EFNB2 in fibroblasts and cocultured these fibroblasts with BCSC1 and BCSC2. Differences of CAF KD and BCSCs in cocultures were assessed using proliferation assays, immunohistochemistry staining of CAF markers and analysis of the niche formation phenotype. The effect of coculture with CAF KD on BCSCs was analyzed using sphere formation assays and Western Blots of key signaling pathways. For *in vivo* experiments, BCSC1 and fibroblasts were orthotopically transplanted in mammary fat pads of mice. Data was analyzed using GraphPad Prism 8, Welch´s t-test.

Results

Downregulation of EphrinB2 expression in CAFs reduced proliferation of CAFs and increased proliferation of BCSCs in coculture. EphrinB2 knockdown also disturbed CAF-BCSC niche formation in coculture and altered CAF marker expression. Upon coculture with CAF KD, self-renewal of BCSCs was reduced. EphrinB2 KD was associated with a decreased STAT3 and increased PI3K signaling in both CAFs and BCSCs after coculture. *In vivo* EphrinB2 knockdown led to an enrichment of BCSCs and CAFs in xenograft tumors.

Conclusion

We postulate that the regulation of EphrinB2 expression in CAFs plays an important role in induction and maintenance of the CAF-BCSC niche and the maintenance of BCSC self-renewal. Therefore, EphrinB2 could thus be a promising additional target in tumor therapy.

1. Background

With 32% of all new cancer diagnoses in women, breast cancer is the most common female cancer. It is still the second leading cause of cancer death for women and the fourth leading cause overall (1). Accounting for 15–20% of all breast cancers, triple-negative breast cancer (TNBC) is a subtype of breast cancer lacking hormone receptor and HER2 receptor expression (2, 3). It is the most aggressive subtype with the lowest 5-year survival rate of 78% and the lowest relapse-free survival time compared to other breast cancer subtypes in every stage (2–6). Furthermore, TNBC is often diagnosed at a later stage and has no targeted treatment options. Instead, it is treated mainly with chemotherapy (4, 5).

Cancer stem cells (CSCs) are a specific population of cells in cancer characterized by self-renewal, dormancy, rapid proliferation, differentiation potential, and the ability to recapitulate the heterogeneity of original tumors. They are associated with maintenance and tumor growth, recurrence, metastasis, resistance and thus a poor prognosis (7–10).

Breast cancer stem cells (BCSCs) used here are primary breast cancer cells, isolated by our lab from TNBC tumors after preoperative chemotherapy treatment (11). BCSC1 is a cell line isolated from a tumor after neoadjuvant treatment with sequential chemotherapy (FEC, FAC, TAC, TC, cisplatin) and was chosen as a representation of heavily treated breast cancer (11, 12). In contrast, BCSC2 is a cell line isolated from a tumor pretreated with only paclitaxel and doxorubicin (11, 12).

Studies have shown that the interaction between CSCs and their tumor microenvironment (TME) may have a role in maintaining the specific characteristics of CSCs (7–9, 13, 14). The main cell type in the TME is cancer-associated fibroblasts (CAFs), a heterogeneous cell type thought to have tumor-promoting as well as tumor-suppressing qualities (8, 15–17). CAFs are involved in tumor progression and resistance by remodeling extracellular matrix, secreting regulatory factors, increasing drug resistance, and inhibiting immune response (14–17). They also induce desmoplasia, increasing tissue stiffness and fibrosis, which is correlated with cancer progression and poor outcome (8, 16–18). It allows tumor cells to migrate and invade through the TME (16, 17) while the increased stiffness of the desmoplastic stroma acts as a physical barrier for chemotherapeutics (16, 17). Targeting CAFs, which maintain the TME and CSC niches, has been postulated as a synergistic addition to traditional treatment (8, 14, 17).

Previous work from our lab revealed a specific niche morphology of CAFs and BCSC when cocultured, referred to as the stromal phenotype of encapsulation (SPE), in which the CAFs formed a tight encapsulation around BCSC clusters at the tumor-stromal interface (19). Differentially expressed genes in CAFs were defined after being cocultured with BCSC1 and BCSC2. One of these genes is EFNB2, which codes for the protein EphrinB2 and was significantly upregulated in fibroblasts after coculture.

EphrinB2 is a transmembrane protein that binds mainly to the receptor EphB4 and plays an important role in developmental processes such as vasculogenesis, neurogenesis, cardiogenesis and fibrosis, as well as proliferation, adhesion and migration (20–23). In cancer, EphB4-EphrinB2 signaling has been

found to act both tumor-promoting as well as tumor-suppressing (24). In CAFs of the prostate, EphrinB activation was found to participate in cancer progression (25).

As increased stromal fibrosis is correlated with cancer progression (16, 18), we investigated the role of the upregulation of EFNB2 in CAFs by inducing a lentiviral knockdown in fibroblasts, followed by coculturing them with BCSCs.

A decreased EphrinB2 expression in CAFs disrupted the tight CAF encapsulation of BCSC clusters, leading to a higher proliferation but a reduced self-renewal capacity of BCSCs in these cocultures. *In vivo* EphrinB2 knockdown led to an enrichment of BCSCs and CAFs in xenograft tumors.

2. Materials and Methods

2.1 Cell culture

BCSCs are primary triple-negative breast cancer cell lines previously isolated and published by our lab (11, 12, 26). These cells were expanded in 60mm dishes which were coated beforehand with 1ml of 98% MSC + R (MSC: Mammary stem cell medium (11) and R: 0.0005% RhoKinase, Calbiochem 555552) and 2% Cultrex (R&D 3433-010-01) and incubated 30min at 37°C. The cells were cultured with 5ml MSC + R at 37°C under hypoxic conditions with 92% N_2, 5% CO_2, and 3% O_2. Medium was changed twice a week.

Cells were passaged once a week. They were washed with 1x PBS (Gibco 70011-036) and detached using 1ml Accutase® (Sigma-Aldrich A6964) in which they were incubated at 37°C for 20 minutes. Afterwards, the Accutase® was diluted using MSC in a 1:1 ratio. Cells were then pelleted by centrifugation at 200 rcf for 3 min. The supernatant was discarded, cells resuspended in PBS and counted using a Neubauer chamber. The needed number of cells was seeded again on a coated dish. BCSC lines were used up to passage 35.

Fibroblasts (human neonatal foreskin fibroblasts, MTI GlobalStem, GSC-3002) were cultured in T75 flasks with 10ml DMEM (Gibco 41966-029) containing 10% FBS (Gibco 10500-064) and 1% Penicillin-Streptomycin (Gibco 15140-122). These cells were incubated at 37°C and medium was changed once a week. The knockdown as well as scramble fibroblasts were cultured with 1200µg/ml geneticindisulphate (G418; Roth CP11.2) to inhibit overgrowth of cells without the knockdown.

Fibroblasts were passaged in the same way as the BCSCs. After incubating with Accutase for 10min at 37°C, centrifugation for 3 minutes at 200rcf, resuspension in DMEM + 10% FBS + 1%, Penicillin-Streptomycin and counting, the needed cells were seeded again with DMEM. The fibroblasts were used up to passage 10.

2.2 Cocultures

BCSC1 and BCSC2 were cocultured with fibroblasts in a ratio of 1:1, 1:2, 1:5 or 1:10. For this, the monocultures were harvested and counted as described above. Depending on the amount needed, cells

were mixed in according ratios in 1,5ml Eppendorf Tubes and then seeded on previously coated wells or dishes. Cocultures were incubated at 37°C in hypoxia.

For 96-well plates, the wells were coated with MSC + R and 2% Cultrex beforehand. For a ratio of 1:10 300 BCSCs and 2,7K fibroblasts were seeded per well (total number of 3K cells/well with 200µl MSC + R). For a ratio of 1:5 600 BCSCs and 2,4K Fibroblasts were seeded per well. After 1 day, G418 was added (1200µg/ml) and medium was changed every two days.

For 384-well plates, the wells were coated with MSC + R and 2% Cultrex and cocultures were seeded in a ratio of 1:10 (200 BCSCs and 1,8K fibroblasts/ well) in 60µl MSC + R. For 100mm dishes were coated and BCSC1 cocultures were seeded in a ratio of 1:1 (90K BCSCs and 90K fibroblasts) while BCSC2 cocultures were seeded in 1:1,5 ratio (70K BCSCs and 110K fibroblasts) with 10ml MSC + R. Medium was changed twice a week. Cocultures with knockdown or scramble fibroblasts were cultured with G418.

2.3 Measurement of Density of Fibroblasts

To measure the density of the fibroblasts (scramble or knockdown) in cocultures with BCSCs, cells were seeded in 96-well plates in a 1:10 ratio and imaged after 8 days via IncuCyte® S3 (Sartorius 4647) at 20x magnification. Next, the integrated density of the fibroblasts (cytoplasmic mCherry tagged) was measured. To do this, the integrated density per area (IntDen/area) of randomly selected, defined areas near and far from the BCSC clusters were calculated using ImageJ. The IntDen/area of the fibroblasts near the BCSC clusters was compared to the Int/Den of the fibroblasts far from the BCSC clusters. The higher the IntDen/area measured the higher the density of the fibroblasts is in this area, as there is then a higher amount of fibroblasts with condensed cytoplasm per area. When comparing the IntDen/area of the BCSC-cluster near fibroblasts to the BCSC-cluster far fibroblasts a higher number indicates a larger difference between these areas, thus a stronger CAF-like morphology of the fibroblasts near the BCSC clusters (Suppl. Figure 3).

2.4 Fluorescence activated cell sorting

BCSCs and fibroblasts were seeded in cocultures on 100mm dishes as described above and grown for about 7 days. Next, the cells were detached, washed with 1xPBS and resuspended in PBS + 2% FBS. The cells were then transferred into FACS tubes via 35µm strainer. Cells were sorted via GFP signal, the BCSCs being GFP positive and the fibroblasts GFP negative, in the Flow Cytometry Facility of the Interdisciplinary Center for Clinical Research (IZKF) Faculty of Medicine at RWTH Aachen University. For cell sorting the BD FACSAria™ Fusion equipped with 5 lasers and a configuration for up to 18 fluorescent parameters (3–6–2–4–3)) with the BD FACSDIVA Software Version 9.4 (BD Biosciences, San Jose, CA, USA) was used.

2.5 Lentiviral Knockdown

Suppl. Table 2 shows the plasmids used for lentiviral transduction. For the preparation of lentivirus HEK293T cells (Invitrogen, RRID: CVCL_6911, Thermo Fisher, Waltham, MA, USA) were used. The helper

packaging plasmid mix was created by adding 700ng CMVdR 8.74 (Addgene, 22036, Watertown, MA, USA; 5200.4ng/µl) and 350ng pMDVSVG (Addgene, 8454, Watertown, MA, USA; 4419.6ng/µl) for each well needed in an 1,5ml tube. In another tube 4µl X-tremeGENE™ HP DNA Transfection Reagent (Sigma-Aldrich, 6366236001, Taufkirchen, Germany) and 400µl Opti-MEM(Life Technologies, 11058021, Carlsbad, CA, USA) per well were mixed and added to the packaging plasmid mix. 1000ng/well were spotted into each well of a 6-well plate, 3 plates in total. Next, 400µl of the helper plasmid packaging mix was added into each well and incubated for 30 minutes at room temperature. HEK293T cells (2x 10^6 cells/ well) were seeded in 1600µl medium (DMEM + 10%FBS + 1% Penicillin/Streptomycin) in each well. After 24 hours the medium was changed with 2ml MSC/ well. After additional 24 hours the viral supernatant (2ml/well, 18 wells in total) was collected and centrifuged at 500g at room temperature for 10 minutes. The supernatant was collected and filtered (0.45µm; Whatman WH10462100). The viral supernatant was overlayed on the sucrose-containing buffer (50mM Tris-HCl pH 7.4, 100mM NaCl, 0.5mM EDTA, 10% sucrose; filtered to sterilize) in a ratio of viral supernatant 4:1 buffer, carefully inverted to mix and then aliquoted in 5ml tubes and centrifuged at 10 000g and 4°C for 4 hours. The supernatant was removed and discarded, the remaining virus pellets resuspended in 500µl MSC and dispatched in 1,5ml tubes. 2ml of fresh MSC was added to the HEK293T cells and the viral supernatant collected after additional 24h. Previous steps were repeated to gather day 2 virus. The virus was stored at -80°C. The lentivirus was titrated on fibroblasts to determine the amount of virus particles/µl MSC.

To transduce the wanted cells, cells were seeded in 6-well dish. After 24 hours the virus was added as well as medium with 0.15% polybrene (Sigma-Aldrich 107689). BCSCs were transduced with a multiplicity of infection (MOI) of 10, fibroblasts with a MOI of 1. The cells were centrifuged at 1000g at room temperature for 1 hour. After 24 hours the media was changed to remove the virus. After 24 additional hours the antibiotic (G418; 1200µg/ml for fibroblasts, 750µg/ml for BCSC1, 600µg/ml for BCSC2) was added to select transduced cells.

2.6 Proliferation assay

Cells were harvested and counted as described above and then seeded in 96-well plates (3K BCSCs/ well or 2K fibroblasts/ well). For BCSCs or cocultures, the wells were coated with 40µl beforehand. Media was changed every 2 days. The cells were imaged using IncuCyte® S3 every 6 hours for up to 7 days. Increase of confluence or fluorescent area over time was analyzed using IncuCyte® Live-Cell analysis system.

2.7 Protein Isolation and Western Blot

Cells were harvested as previously described or used directly after FACS cell sorting. Cells were pelleted at 200rcf for 3 minutes and washed with PBS. After taking off the supernatant, pellets were stored at -80°C.

For protein isolation the pellets were lysed using RIPA-lysis buffer (ThermoFisher 89900) + cOmplete™ protease inhibitor (Merck 11697498001) + PhosSTOP™ (Merck 4906845001), with which they were incubated for 30 minutes on ice and afterwards centrifuged at 13000rpm and 4°C for 15 minutes. The

supernatant was transferred into new 1,5ml Eppis. Protein concentration was quantified using DC™ Protein Assay Kit II (Bio-Rad 5000112) and measured via SpectraMax iD3 (Molecular Devices) of the IZKF. Isolated proteins were diluted in 90% Laemmli Sample buffer (BioRad 1610747) and 10% ß-mercaptoethanol to the desired concentration and incubated at 95°C for 5 minutes.

For Western blotting, 10 to 15µl of protein solution were loaded in each well of the gels (Any kD™ Mini-PROTEAN® TGX™ Precast Protein Gels, 15-well, 15µl; Bio-Rad 4569036 and 10-well, 30µl Bio-Rad 4561033) in the Mini-PROTEAN® Tetra Vertical Electrophoresis Cell chamber with running buffer (3g Tris, 14.4g glycin, 1g SDS in 1l distilled water). The gel was run at 130V for 1 ½ hours and then transferred onto the membrane (Trans-Blot Turbo Mini 0.2 µm PVDF Transfer Packs, Bio-Rad 1704156) via Trans-Blot® Turbo Transfer System (Biorad 1704150). Afterwards the membranes were blocked for 1 hour at room temperature using TBST (2.4g Tris, 8.8g NaCl, pH 7.6, 1ml Tween-20 in 1l distilled water) with 5% BSA. The membrane was then incubated at 4°C overnight with the primary antibody diluted in TBST with 5% BSA (anti-EphrinB2: Antikoerper online ABIN1867699 1:500, anti-EphB4 Cell Signaling Technology 14960S 1:500, anti-ß-actin Sigma Aldrich A5441 1:2000, anti-GAPDH Cell Signaling Technology 8884S 1:2000, anti-STAT3 Cell Signaling Technology 4904S 1:1000, anti-PI3K Cell Signaling Technology 13666S 1:1000) on a rocking shaker. The next day membranes were washed 3x for 5min with TBST on the rocking shaker. The membranes were incubated with the secondary antibody diluted in TBST with 5% BSA (polyclonal rabbit anti-mouse 1:2000 Dako P0260; polyclonal goat anti-rabbit 1:2000, Dako P044801) for 1 hour at room temperature. Afterwards the membranes were washed again 3x for 5 minutes with TBST. To detect the bands, membranes were coated with Miracle-Star™ WB detection system (iNtRON Biotechnology 16028) and detected using the Vilber Lourmat Fusion SL. The images were quantified using ImageJ.

For stripping of bands, membranes were incubated for 45 minutes at 50°C in harsh stripping buffer (20ml SDS 10%, 12.5ml 0.5M Tris HCl pH6.8, 67.5ml distilled water, 0.8 ml β-mercaptoethanol) and afterwards washed 5x for 5 minutes with distilled water on the rolling shaker. Afterwards the membranes were blocked for 1 hour at room temperature using TBST with 5% BSA and then incubated with the primary antibody overnight at 4°C

2.8 Sphere formation assay

Cells were harvested as described or used after FACS cell sorting. Cells were counted and 200 cells/well were seeded in 20µl MSC + R 1:1 Cultrex in a 96-well Clear Flat Bottom Ultra-Low Attachment Microplate (Corning 3474). Six wells were seeded per cell line. After 20 minutes incubation at 37°C 150µl MSC + R were added. The plate was incubated at 37°C in a hypoxia chamber and after 7 days 30µl MSC + R was added to each well. After 10 days the number of spheres formed were counted.

2.9 Chemosensitivity assay

BCSCs and FB Scr or FB KD were seeded on mono- or coculture (ratio of 1:10) in 384-well plates as described above. After 1 day, paclitaxel or doxorubicin as well as G418 were added to a final

concentration of 1, 3 and 10ng/ml (paclitaxel) or 10, 20, 30ng/ml (doxorubicin). Cell proliferation was imaged and measured every 6 hours using IncuCyte® S3.

2.10 Immunofluorescence staining

Cocultures of BCSCs and fibroblasts (scrambled or knockdown) were seeded in a ratio of 1:2 (1,3K BCSCs and 2,7K fibroblasts, total of 4K/well) and 1:5 (800 BCSCs and 3,2K fibroblasts, total of 4K/well) in a 96-well plate as previously described and medium changed every two days. After 5 to 7 days the plates were washed 2x with PBS and then fixated with 200µl ice-cold methanol/well. The plates were covered with parafilm and stored at -20°C.

To stain the cells, wells were washed 2x with PBS for 3 minutes, then the cells were permeabilized with TBST (20mM Tris, 150mM NaCl, 0.05% Tween-20) 3x for 2 minutes. Afterwards, the wells were washed 1x with ovalbumin/PBS 1mg/ml (ova/PBS) (ovalbumin: Merck A5503-5G) and blocked with 100µl ova/PBS per well for 1 hour at room temperature. Next, the ova/PBS was removed and 40µl primary antibody added. Vimentin (GeneTex GTX16700) was diluted 1:200 in ova/PBS and FAP (Invitrogen pa5 99313) diluted 1:250 in ova/PBS. The plate was covered with parafilm and incubated at 4°C overnight. The next day the wells were washed 3x for 5 minutes with PBS and blocked with 50µl ova/PBS for 10 minutes. The cells were incubated with 50µl of secondary antibody anti-rabbit Alexa Fluor 488 (Life technologies A21206), diluted 1:500 in ova/PBS at 37°C for 30 minutes. Wells were then washed 3x for 5 minutes with PBS and 100µl/ well of 1x DAPI staining buffer (10x nuclei staining buffer: 100mM tris-HCl, pH7.4; 100mM EDTA, 1M NaCl and filled up to 50ml with distilled H_2O) with 0.1µg/ml DAPI was added. Staining was imaged and analyzed at 20x magnification using the IncuCyte®.

2.11 Orthotopic Xenografts in Mice

The *in vivo* experiments on NOD/SCID mice (8 weeks old, purchased from Janvier Labs, Le Genest-Saint-Isle, France) were done in accordance with German Animal Welfare regulations, IACUC conform and approved by the local authorities (LAVE: Landesamt für Verbraucherschutz und Ernährung NRW; 2024-630-Grundantrag). 4 mice were transplanted BCSC1 and FB Scr and 4 mice were transplanted BCSC1 and FB KD. After anesthesia with isoflurane, shaving of the abdomen and desinfection with beta-isodona as well as 70% ethanol a small y-shaped incision was performed and the fifth mammary fat pad exposed. The cell mixture, 50K BCSC1 and 250K fibroblasts in 40µl MSC + R and Matrigel 1:1 (Corning® Matrigel® Growth Factor Reduced (GFR) Basement Membrane Matrix 354230), was injected directly into the mammary fat pad on both sides. The incision was then closed using staples (AutoClip® System 12020-00). Mice were monitored daily and tumor growth was measured twice a week. Mice were sacrificed before tumor diameter reached 15mm. Mice were euthanized by cervical dislocation by trained personnel as approved in our animal procedural protocol, a method selected to ensure rapid death while minimizing the use of additional anesthetic agents. Tumors and organs were excised, weighed and fixated in 4% PFA.

2.12 Immunohistochemistry

The staining was performed by the lab technician Anja Steinle. Mice were orthotopically transplanted with BCSCs and non-irradiated human fibroblasts. After excision the tumors were fixated using methanol or 4% PFA, then washed with increasing concentrations of ethanol (70%, 80%, 90%, 96%), transferred into xylene to displace the ethanol, then transferred to and embedded in molten paraffin (60–65°C). The block of paraffin was cut into 4–10µm thick slices and placed on glass slides. For staining of the slides, they were incubated at 37°C overnight. Slides were washed 3x with xylene for 10 minutes, then with decreasing (100%, 96%, 70%, 50%) ethanol concentrations and finally for 5 minutes with running distilled water. The slides were microwaved in 50µl citrate buffer, pH6 for 30 seconds at 800W, placed in a water bath for 1 hour at 97°C and allowed to cool down for 15 minutes. Slides were washed for 5 minutes under running distilled water and the endogenous peroxidase was blocked with 5% H_2O_2-methanol for 15 minutes. After washing with distilled water, the slides were incubated in TBST (cell signaling 9997S). Slides were blocked with 150µl 7% milk powder in TBST for 1 hour and incubated overnight at 4°C with 150µl primary antibody diluted in antibody diluent (Dako Agilent S302283-2): anti-EphrinB2 (Antikoerper online ABIN1867699 1:200, Anti-alpha SMA antibodies.com A82445 1:100, anti-GFP Invitrogen A-11122 1:200, anti CD31 Invitrogen PA5-32321 1:100). The next day the slides were washed 3x with TBST and then incubated for 45 minutes at room temperature with the secondary antibodies (polyclonal goat anti-rabbit immunoglobulins/HRP: Dako Agilent P044801 1:100; polyclonal rabbit anti-goat immunoglobulins/HRP: Dako Agilent P0449 1:100). Afterwards slides were washed 3x with TBST and 150µl diaminobenzidine (DAB-Kit Dako-Agilent K346811-2) added for 9 minutes at room temperature. After washing with distilled water, slides were counterstained with hematoxylin (Dako Agilent, CS70030-2) for 10 minutes and then rinsed with distilled water for 10 minutes. Afterwards the slides were washed with increasing ethanol concentrations (70%, 96%, 100%). Slides were immersed in xylene, covered with 1–2 drops of Entellan (Sigma-Aldrich 107961) and a coverslip and allowed to dry overnight. The slides were imaged with Echo microscope (Echo Rebel, Workhorse Microscope for Brightfield/Tissue Culture).

2.13 Analysis of Immunohistochemistry

Analysis of the stainings was performed by pathologist Dr. med Roman Bülow. Whole slide images (WSI) were acquired using a Hamamatsu S360MD scanner at 40x resolution. All subsequent digital analyses were performed using QuPath v0.6.0 and custom R scripts (R version 4.3.0). Rectangular regions of interest (ROIs) of equal sizes were automatically placed at the center of each tissue core using a custom QuPath script. Cell nuclei were detected using InstanSeg, (model version 0.1.0). The segmentation pipeline utilized three input channels (RGB) with 512×512-pixel tiles and 32-pixel inter-tile padding to ensure accurate detection at tile boundaries. Automatic threshold determination was implemented using Otsu's method, which optimally separates bimodal distributions by minimizing intra-class variance. This approach identifies natural population boundaries in the DAB staining intensity distribution. Alternative thresholding methods (Triangle, Li, Moments) were evaluated to ensure robustness of classification. Cells were classified as "Positive" or "Negative" based on nuclear DAB optical density measurements relative to the calculated threshold. Necrotic regions were manually annotated in all WSIs by a trained observer. The necrotic area fraction was calculated as the ratio of necrotic tissue area to total tissue area (tumor + necrosis) for each image. This provided a quantitative assessment of tissue viability

across treatment groups. Data from multiple sections per animal were aggregated to account for technical replicates. To account for the hierarchical structure of the data (multiple cells nested within sections, multiple sections per animal), mixed-effects logistic regression models were employed using the lme4 package. Animal identifier was included as a random effect to control for inter-animal variability. The primary outcome was the proportion of positively stained cells. For animal-level comparisons, mean positive cell percentages were calculated per animal. Between-group differences were assessed using Student's t-test when data met normality assumptions (Shapiro-Wilk test, $p > 0.05$) or Mann-Whitney U test for non-parametric data. Effect sizes were calculated using Cohen's d for parametric comparisons. For necrosis analysis, a linear mixed-effects model was fitted with group and staining type as fixed effects and animal identifier as a random effect. Post-hoc pairwise comparisons were performed using estimated marginal means (emmeans package) with Tukey adjustment for multiple comparisons. All automated measurements underwent quality control checks including: (1) verification of successful cell segmentation through visual inspection of random samples, (2) confirmation of threshold stability across technical replicates, and (3) assessment of measurement distributions for outliers or technical artifacts. All analyses were performed using QuPath v0.6.0 for image analysis and R v4.3.0 for statistical analysis. Custom scripts were developed to ensure reproducibility and are available upon request. Key R packages included: dplyr for data manipulation, ggplot2 for visualization, lme4 for mixed-effects modeling and emmeans for post-hoc comparisons.

2.14 Statistical Analysis

Biological repeats are indicated as n-value. Data was analyzed using GraphPad Prism 8, Welch´s t-test. Data is shown as mean ± SEM. Statistical significance was defined as a p-value < 0.05. (*) is defined as $p < 0.05$; (**) is defined as $p < 0.01$; (***) is defined as $p < 0.001$; (****) is defined as $p < 0.0001$.

3. Results

3.1 EphrinB2 is upregulated in CAFs in breast cancer

GFP-tagged BCSC1 and BCSC2 were cocultured with wildtype fibroblasts and then sorted via FACS. After MACE-sequencing and analysis of differently expressed genes EFNB2 was discovered as an upregulated gene in CAFs (Image created with BioRender).

To recapitulate the specific phenotype of fibroblasts in coculture with BCSCs described by Muralidharan et al. (19), we cocultured BCSC1 and BCSC2 with wildtype fibroblasts (FB WT) in a 1:5 and 1:10 ratio, respectively. BCSCs formed clusters, encapsulated by dense streams of fibroblasts directly around these clusters. Fibroblasts farther away from BCSC clusters formed a looser pattern (Fig. 2a). This corresponds to the findings described by Muralidharan et al. (19).

RNA levels indicated an upregulation of the EFNB2 gene which was also confirmed on protein level (Fig. 2b). We cocultured BCSC1 and BCSC2 with wildtype fibroblasts (FB WT) for 7 days and then sorted the cells by FACS. EphrinB2 expression in fibroblasts before coculture (FB WT) and in fibroblasts after

coculture with BCSC1 (CAF1) or BCSC2 (CAF2) was detected and quantified by Western blot. In CAF1 and CAF2, EphrinB2 expression increased after coculture with BCSCs (Fig. 2b). Upregulation of EphrinB2 was permanent for up to 3 passages following FACS separation (Suppl. Figure 1a).

Since EphB4 is the preferred receptor of EphrinB2, we analyzed EphB4 expression in BCSC1 and BCSC2 after CAF-coculture. In both cell lines, EphB4 was upregulated (Fig. 2c). However, upregulation of EphB4 was only stable in BCSC2 in later passages, while EphB4 expression in BCSC1 decreased over time (Suppl. Figure 1b).

This increase in EphrinB2 expression could also be detected *in vivo*. Immunohistochemical analysis of normal breast tissue compared to BCSC1 and BCSC2 tumors from orthotopic xenografts showed a strong EphrinB2 expression not only in the BCSCs themselves but also in the CAFs surrounding the cancer cells (Fig. 2d).

Taken together, we observed increased EphrinB2 expression and its receptor EphB4 *in vitro* in BCSC-fibroblast cocultures and *in vivo* in xenograft mice models.

a) Cocultures of BCSC1 (GFP) or BCSC2 (GFP) with fibroblasts (FB WT, mCherry) in a ratio of 1:10 and 1:5, 10x magnification with IncuCyte®. Scalebar represents 400 µm **b)** Western blot and quantification of EphrinB2 in fibroblasts before (FB WT) and after coculture and FACS sort with BCSC1 (CAF1) and BCSC2 (CAF2) n = 3, mean **c)** Western blot and quantification of EphB4 in BCSCs before and after coculture (a. Cc) and FACS sort with FB WT n = 3, mean d) Staining of EphrinB2 in normal breast tissue (left), murine tumor with BCSC1 and fibroblasts (middle) and murine tumor with BCSC2 and fibroblasts (right). Black arrows indicate EphrinB2-expressing CAFs.

3.2 Knockdown of EphrinB2 in fibroblasts disturbs stromal phenotype of encapsulation and changes the niche dynamic

To investigate the role of EphrinB2 further, we created EphrinB2 knockdown fibroblasts (FB KD) through lentiviral transduction of shRNA. The knockdown was confirmed and quantified by Western blotting (Fig. 3a). As a control, fibroblasts were transduced with scramble shRNA (FB Scr). The knockdown in the fibroblasts was stable over several passages (Suppl. Figure 2)

As previously described, fibroblasts form a tight encapsulation around clusters of BCSCs in coculture, the stromal phenotype of encapsulation (19). This specific phenotype is altered when BCSCs are cocultured with knockdown fibroblasts. The dense streams of the CAFs directly surrounding the BCSC clusters are reduced, and thus less CAF-like. Instead, the density of fibroblasts near and far from BCSC clusters is more equal (Fig. 3b). To quantify this observation, cocultures of BCSC1 and BCSC2 with FB Scr and FB KD were analyzed (Fig. 3c, Suppl. Figure 3). There was a clear reduction of the stromal phenotype of encapsulation (Fig. 3d). These findings indicate that CAF-specific encapsulation of the BCSC clusters was disturbed upon EphrinB2 knockdown.

To further characterize the effects of EphrinB2 knockdown in the fibroblasts, proliferation was analyzed. No differences were observed in FB Scr and FB KD monocultures (Fig. 3e). On the contrary, in coculture with BCSC1 and BCSC2 the proliferation of FB KD reduced (Fig. 3f). Proliferation of BCSCs in these cocultures was increased (Fig. 3g). This phenomenon could be confirmed in varying ratios with BCSC1 and BCSC2 (Suppl. Figure 4a, 4b).

a) Western blot and quantification of EFNB2 knockdown in fibroblasts (FB KD) compared to control (FB Scr) n = 3 mean ± SEM, p = 0.0078 **b)** With control fibroblasts CAFs encapsulate the BCSC clusters tightly, with EFNB2 knockdown in fibroblasts this encapsulation is reduced (Images created with BioRender). **c)** Representative images of cocultures with BCSC1 or BCSC2 and FB Scr or FB KD in a ratio of 1:10, 20x magnification with IncuCyte® Scalebar represents 200µm **d)** Relative density of fibroblasts BCSC-cluster near compared to the relative density of fibroblasts cluster far, in coculture with BCSC1 (top) or BCSC2 (bottom), ratio 1:10 n > 20 mean ± SEM BCSC2: p = 0.009 **e)** Proliferation of FB Scr and FB KD in monoculture n = 4 mean ± SEM **f)** Proliferation of FB Scr and FB KD in coculture with BCSC1 (left) and BCSC2 (right) ratio 1:10 n = 3 mean ± SEM **g)** Proliferation of BCSC1 (left) and BCSC2 (right) in coculture with FB Scr or FB KD ratio 1:10 n = 3 mean ± SEM.. (*) is defined as $p < 0.05$; (**) is defined as $p < 0.01$; (***) is defined as $p < 0.001$; (****) is defined as $p < 0.0001$.

3.3 EphrinB2 knockdown in fibroblasts increases Vimentin and decreases FAP expression

To further characterize these changes, we analyzed CAF marker expression in knockdown fibroblasts. Immunohistochemistry revealed an upregulation of Vimentin in FB KD cocultures with BCSC1 and BCSC2 compared to FB Scr (Fig. 4a). When quantifying FAP expression in the CAFs, no differences were observed in cocultures with BCSC1 and a slight decrease was observed in BCSC2 (Fig. 4b).

3.4 Coculture with knockdown-fibroblasts leads to reduced self-renewal in BCSCs

We wanted to investigate what influence knockdown fibroblasts have on BCSC stemness and maintenance of the stem cell phenotype. GFP-tagged BCSC1 and BCSC2 were cocultured with FB Scr or FB KD for 7 days. Afterwards the cells were separated via FACS and the BCSCs were introduced in sphere forming assays. Here, BCSCs that had been cocultured with FB KD (BCSC + FB KD) showed a significant reduction in the number of spheres formed compared to the BCSCs who had been cocultured with FB Scr (BCSC + FB Scr) (Fig. 5a, b). This was true for both BCSC lines. Thus, we concluded that the interaction between fibroblasts and BCSCs has an impact on self-renewal of BCSCs and is impacted when EphrinB2 expression is reduced in fibroblasts.

To investigate signaling pathways associated with EphrinB2-mediated signaling and fibroblast activation, we analyzed the expression of STAT3 and PI3K in both BCSCs and fibroblasts following coculture.

STAT3 expression was consistently reduced in BCSC1 and BCSC2 after coculture with FB KD compared to FB Scr controls. Likewise, STAT3 levels were decreased in CAF1 KD and CAF2 KD, with the strongest reduction observed in CAF1 KD. In contrast, PI3K expression was modestly increased in both BCSCs after coculture with FB KD and in EphrinB2-knockdown CAFs compared to their respective controls (Fig. 5c, d).

a) Representative images and quantification of Vimentin staining in cocultures of BCSC1 or BCSC2 with knockdown or scramble fibroblasts in a ratio of 1:2, 20x magnification, imaging and analysis with IncuCyte® n = 3 mean ± SEM BCSC2: p = 0.0222. Scalebar represents 200µm **b)** Representative images and quantification of FAP staining in cocultures of BCSC1 or BCSC2 with knockdown or scramble fibroblasts in a ratio of 1:2, 20x magnification, imaging and analysis with IncuCyte® n = 3 mean ± SEM. Scalebar represents 200µm.. (*) is defined as $p < 0.05$; (**) is defined as $p < 0.01$; (***) is defined as $p < 0.001$; (****) is defined as $p < 0.0001$.

a), b) Representative images and quantification of sphere formation assay of BCSC1 (n = 3) and BCSC2 (n = 2) after coculture with FB Scr or FB KD in a 1:2 ratio, FACS sorted and then seeded out again on their own. Scale bar represents 1mm. mean ± SEM BCSC1: $p < 0.0001$, BCSC2: p = 0.0002 **c)** Western blot and quantification of STAT3 and PI3K in BCSC1 and BCSC2 after coculture with FB Scr (BCSC1 + Scr, BCSC2 + Scr) or FB KD (BCSC1 + KD, BCSC2 + KD) and then sorted via FACS, mean n = 3 **d)** Western blot and quantification of STAT3 and PI3K in FB Scr or KD with BCSC1 (CAF1 Scr and CAF1 KD) or BCSC2 (CAF2 Scr and CAF2 KD) and then sorted via FACS, mean n = 3.. (*) is defined as $p < 0.05$; (**) is defined as $p < 0.01$; (***) is defined as $p < 0.001$; (****) is defined as $p < 0.0001$.

3.5 No difference in the chemoresistance of BCSCs in coculture knockdown-fibroblasts was observed

Next, we wanted to investigate differences in chemoresistance. We treated FB Scr and FB KD in mono- and coculture with BCSCs with increasing concentrations of doxorubicin and paclitaxel. The choice of chemotherapeutics and concentration was based on previous work by Li et al (12). FB Scr and FB KD showed no difference regarding sensitivity to doxorubicin but showed a reduced FB KD proliferation with paclitaxel 3 ng/ml and 10ng/ml (Suppl. Figure 5a). The increased proliferation of BCSCs in coculture with FB KD previously described (Fig. 3g) was also present with lower concentrations of doxorubicin and paclitaxel (Suppl. Figure 5b-e). Overall, BCSC coculture with FB Scr or FB KD did not appear to affect resistance of BCSCs to chemotherapy (Suppl. Figure 5b-e).

3.6 Orthotopic xenografts with knockdown-fibroblasts show increased tumor weight

We performed orthotopic xenografts of BCSC1 with FB Scr and FB KD, respectively, to examine the effects of EphrinB2 knockdown CAFs in vivo. Tumors with FB KD grew slightly faster than those with FB Scr, although not significantly (Fig. 6a, Suppl. Figure 6a). After 4 weeks mice were sacrificed and the tumors removed and analyzed (Fig. 6b). Tumors with FB KD showed an increased weight compared to

those with FB Scr (Fig. 6c). We also measured tumor area based on their largest circumference. There was no significant difference in tumor area between FB Scr and FB KD tumors (Suppl. Figure 6b).

a) Tumor growth in mm over time. BCSC1 and FB Scr or BCSC1 and FB KD were orthotopically transplanted into mammary fat pads of mice in a ratio of 1:5. Diameters of tumors were measured twice a week. n = 8 mean ± SEM **b)** Images of tumors after autopsy. n = 8, ruler for scale **c)** Weight of mouse tumors after autopsy. n = 8 mean ± SEM

3.7 *Tumors with knockdown-fibroblasts consist of a higher amount of BCSCs and CAFs*

Using immunohistochemical analysis we quantified necrotic area of the tumors. No significant difference in necrosis was found between the tumors with BCSC1 and FB Scr or FB KD (Fig. 7a). But tumors with BCSC1 and FB KD showed a higher amount of BCSCs compared to BCSC1 and FB Scr (Fig. 7b). To quantify the number of CAFs in the tumors, we quantified for α-SMA. The tumors with BCSC1 and FB KD also showed a higher number of CAFs than the tumors consisting of BCSC1 and FB Scr (Fig. 7c). To investigate differences in vasculature between the tumors, we stained and quantified the tumors for CD31, a marker for endothelial cells. No difference was observed between the tumors with FB KD and FB Scr (Suppl. Figure 7)

a) Representative images and quantification of necrosis area relative to tumor area, three images per tumor were analyzed, eight tumors per group. Scale bar represents 1mm **b)** Representative images and quantification of immunohistochemistry staining of GFP, so of the BCSCs in murine tumors consisting of BCSC1 and FB Scr or FB KD n = 8 Scalebar represents 200µm **c)** Representative images and quantification of immunohistochemistry staining of SMA, so of the CAFs in murine tumors consisting of BCSC1 and FB Scr or FB KD n = 8. Scalebar represents 200µm

4. Discussion

Cancer-associated fibroblasts are the main cell type in the tumor microenvironment with tumor-promoting qualities. In this study we investigated the effects of EFNB2 regulation in these CAFs upon coculture with BCSCs.

When cocultured with BCSCs, fibroblasts tightly encapsulate the BCSC clusters directly at the tumor-stromal interface. Knockdown of EphrinB2 in CAFs disturbed this encapsulation of BCSCs, instead displaying a looser growth pattern. The encapsulation by CAFs has also been observed in other cancer types and described not as only a passive barrier, but also as an active compression of the tumor cells clusters by CAFs, which is postulated to decrease cancer cells proliferation but also promote stemness, resistance to drugs and metastatic traits (27). Consistent with these studies, BCSCs proliferated faster in coculture with the CAF KDs, so in the cocultures with reduced stromal encapsulation. These proliferation differences were transient without lasting effects in BCSCs after being separated and seeded in monoculture. This suggests that these proliferation differences were a result of EphrinB2-dependant

direct cancer cell-stroma interaction and differences in BCSC encapsulation. In the nervous system, Ephrin/EphB4 signalling was found to elicit contact-mediated repulsion of cells, generating patterns of cell organisation and preventing the intermingeling or invasion of different cell populations (28–30). This could be one mechanism leading to the formation of encapsuled BCSC clusters in the cocultures with CAFs with EFNB2 upregulation. After KD of EphrinB2 in CAFs, this signalling is decreased and the cell organisation pattern disrupted.

In previous studies, CAFs were found to impair doxorubicin-dependent apoptosis and ferroptosis in TNBC cells (31, 32) as well as promote paclitaxel resistance (33, 34). Although we saw differences in encapsulation of BCSC clusters, thus differences in the active compression of cancer cells, we didn´t observe the expected differences in chemotherapy resistance of BCSCs in these cocultures. This could be explained by the use of our BCSC lines, rather than commercial breast cell cancer lines used in other studies. CSCs are known to have an intrinsic resistance to chemotherapy through increased expression of transporter molecules, enhanced repair mechanisms, altered cell cycles and dysregulated apoptosis compared to cancer cells and can even be enriched after chemotherapy exposure (35–37). Additionally, our BCSCs lines were isolated from tumors after exposure to multiple chemotherapies (11, 12), meaning they had already undergone a selection process in the patient. Our chemotherapy choice and concentration was based on previous studies of BCSC1 and BCSC2 in monoculture (12). It is possible that CAF-mediated differences in chemotherapy sensitivity would be observable with a different drug choice, concentrations or exposure time. We did observe differences in chemoresistance of the fibroblasts themselves, with the FB KD being more sensitive, especially to paclitaxel. As CAFs have been shown to be more chemoresistant compared to normal fibroblasts in vitro (14, 38), increased chemotherapy sensitivity could be an indicator that EphrinB2 KD CAFS are a less CAF-like and loose this feature. This could indicate that other CAF-specific functions, especially their tumor supporting ones, could also be impaired.

Knockdown of EphrinB2 in CAFs had opposing effects on the CAF markers, as we observed a higher expression of Vimentin and a slightly lower expression of FAP in coculture. Vimentin was associated with cell motility, structure and integrity and EMT in vitro, shorter overall survival rate and metastasis in vivo (15, 39–41), while FAP was associated with ECM remodeling, fibrogenesis, tumor progression, metastasis and immunevasion in vitro and a worse prognosis and shorter overall survival in cancer patients (15, 42). Our findings indicate a more mesechymal and motile phenotype of EphrinB2 KD CAFs with altered ECM remodeling and fibrogenesis. Further research clarifying exact differences regarding these characteristics and its impact on tumor progression is ongoing.

EphrinB2-mediated encapsulation has a tumor-promoting effect as active compression of cancer cells by CAFs promotes stemness (27). Self-renewal, a hallmark of stemness of CSCs, is root of cancer development and progression, therefore supporting cancer growth, metastasis and therapy resistance (8, 9, 43). Disruption of encapsulation and compression in BCSC and CAF KD cocultures lead to a reduced self-renewal capacity, thus directly impacting stemness of these BCSCs. The JAK/STAT3 pathway was found to be vital to sustaining the proinvasive profibrotic CAF phenotype, increasing

transformation, invasion, self-renewal of CSCs and is linked to a shorter survival (8, 16, 21, 22, 44, 45). We found a reduced STAT3 expression in BCSCs after coculture with EphrinB2 KD CAF with reduced self-renewal. This suggests that EphrinB2 plays a role in CAF-specific signaling pathways e.g. STAT3, as its KD reduced the protein expression in CAFs and BCSCs. The reduced STAT3 expression in BCSCs provides an explanation on a protein level for the reduced self-renewal we observed. It was found that EphrinB2/EphB4 reverse signalling maintained self-renewal of bone marrow mesenchymal stem cells (46). Reduced EphrinB2/EphB4 signalling could be an additional mechanism reducing the self-renewal of BCSCs. Current cancer therapies mainly target rapidly dividing cells and not CSCs, meaning these cells survive and lead to resistance, recurrence and metastasis (9). Targeting self-renewal could limit this tumor growth and thus be an additional tumor treatment option (7).

PI3K signaling is part of the forward signaling EphrinB2/EphB4 pathway, inducing migration and proliferation (22, 23). In colorectal cancer, CAFs were found to induce a slow-cycling state of CSCs with a slower S-phase entry through lower PI3K signalling, making the CSCs less vunerable to chemotherapy (47). This is in line with our observation of increased PI3K signaling in CAF KD and the corresponding BCSCs and increased proliferation of these BCSCs in coculture. It suggests that the EphrinB2 KD CAFs reduce slow-cycling CSCs, explaining the increased proliferation of BCSCs in these cocultures. It furthermore supports our hypothesis that the KD of EphrinB2 in fibroblasts reduces their CAF specific tumor-promoting functions. Our findings contrast with some previous studies, which related PI3K activation to enhanced BCSCs stemness and chemotherapy resistance (8, 9).

In vivo we observed a slight increase in tumor size of tumors with EphrinB2 KD cells, as well as an increase in BCSC and CAF number in these tumors. This increase in proliferation of the EphrinB2 KD cells does not match to our findings from shortterm cultivation in vitro, which could be the result of the replacement of the human fibroblasts by murine fibroblasts during prolonged tumorgrowth in the animal. EphrinB2 KD was found to increase apoptosis in gastric cancer cells, multiple myeloma cells and nucleus pulposus cells (48–50). Our fibroblasts with EphrinB2 KD have a survival disadvantage and showed a slower proliferation compared to control CAFs in vitro, so there is a high probability that they were replaced quickly by murine fibroblasts in vivo. A continuous knockdown of EphrinB2 in fibroblasts would need to be xenografted into EphrinB2 KD mice, which is impossible due to embryonic lethality (51, 52). Future characterization of KD fibroblasts in xenografts is required to quantify their EphrinB2 expression and determine the functional consequences of its knockdown in vivo.

In previous work looking into the role of upregulated genes and proteins in CAFs, the protein IRF6 was postulated to exert its tumor-promoting effects by supporting BCSC survival and reducing necrosis (19). With EphrinB2 we postulate that it exerts its tumor-promoting effects in CAFs by supporting the tight CSC encapsulation by these CAFs, leading to a decreased BCSC proliferation but an increase in BCSC self-renewal.

5. Conclusion

In this study we investigated the role of EphrinB2 in cancer-associated fibroblasts, as this protein was shown to be upregulated in fibroblasts after coculture with BCSCs. In vitro, CAFs with reduced EphrinB2 expression showed a lower proliferation rate, different CAF marker expression as well as different protein expression of important signalling pathways. Regarding BCSC-CAF coculture morphology, the specific BCSC cluster encapsulation was disrupted and thus also the mechanical compression of BCSCs by CAFs. This and other factors led to a decreased self-renewal of these BCSCs after coculture with the knockdown fibroblasts. The reduction of EphrinB2 signaling in fibroblasts decreased their tumor-supporting CAF-like properties and thus could be an interesting additional target in future breast cancer therapies.

List of abbreviations

BCSC Breast cancer stem cell

CAF Cancer-associated fibroblasts

CAF1 Cancer-associated fibroblasts with BCSC1

CAF2 Cancer-associated fibroblasts with BCSC2

CAF KD Cancer-associated fibroblasts with EphrinB2 knockdown

CAF Scr Cancer-associated fibroblasts scramble

CSC Cancer stem cell

Dox Doxorubicin

ECM Extracellular matrix

EMT Epithelial-mesenchymal transition

FAC 5-Fluorouracil, Adriamycin, Cyclophosphamide

FACS Fluorescence Activated Cell Sorting

FAP Fibroblast Activation Protein

FB Fibroblast

FEC 5-Fluorouracil, Epirubicin, Cyclophosphamide

IRF6 Interferon Regulatory Factor

JAK Januskinase

KD Knockdown

M Passage

Pacli Paclitaxel

PI3K Phosphatidylinositol 3-Kinase

Scr Scramble

SPE Specific Phenotype of Encapsulation

STAT3 Signal Transducer and Activator of Transcription 3

TAC Taxotere, Adriamycin, Cyclophosphamide

TC Taxotere, Cyclophosphamide

TME Tumor Microenvironment

TNBC Triple-Negative Breast Cancer

Declarations

Ethics approval and consent to participate

The animal experiments mice were done in accordance with German Animal Welfare regulations and approved by the local authorities (2024-630-Grundantrag). The maximum tumor size permitted by the ethics committee of 15mm was never exceeded.

Consent for publication

Not applicable.

Competing interests

All authors declare no financial or non-financial competing interests.

Funding

This work was supported by the German Cancer Aid (Deutsche Krebs Hilfe) through the Mildred-Scheel Doctoral Program, funded was Paula Dorsch. Furthermore, it was supported by the DFG through support from the RTG 2375 to PD Dr. Jochen Maurer. The funders played no role in study design, data collection, analysis and interpretation of data, or the writing of this manuscript

Author Contribution

PD, JM were responsible for conceptualization; PD, TH, AS, HM, JM, ES were responsible for methodology; PD, AI, AS, HM were responsible for data acquisition: PD, RB were responsible for statistical analysis, PD was responsible for the manuscript draft; JM was responsible for supervision; TH, LH, JM were responsible for review and editing; PD, JM were responsible for funding acquisition; JM was responsible for project administrationAll authors read and approved the final manuscript.

Acknowledgement

This work was supported by the Flow Cytometry Facility, a core facility of the Interdisciplinary Center for Clinical Research (IZKF) Aachen within the Faculty of Medicine at RWTH Aachen University and by the German Research Foundation (DFG), project ID 439895892

Data Availability

The datasets supporting the conclusions of this article are included within the article and its additional files.

References

1. Siegel RL, Kratzer TB, Giaquinto AN, Sung H, Jemal A, Cancer statistics. 2025. CA: a cancer journal for clinicians. 2025;75(1):10–45.
2. Howard FM, Olopade OI. Epidemiology of Triple-Negative Breast Cancer: A Review. Cancer J (Sudbury Mass). 2021;27(1):8–16.
3. Li X, Yang J, Peng L, Sahin AA, Huo L, Ward KC, et al. Triple-negative breast cancer has worse overall survival and cause-specific survival than non-triple-negative breast cancer. Breast Cancer Res Treat. 2017;161(2):279–87.
4. Giaquinto AN, Sung H, Newman LA, Freedman RA, Smith RA, Star J, et al. Breast cancer statistics 2024. Cancer J Clin. 2024;74(6):477–95.
5. Brenton JD, Carey LA, Ahmed AA, Caldas C. Molecular classification and molecular forecasting of breast cancer: ready for clinical application? J Clin oncology: official J Am Soc Clin Oncol. 2005;23(29):7350–60.
6. Sørlie T, Perou CM, Tibshirani R, Aas T, Geisler S, Johnsen H, et al. Gene expression patterns of breast carcinomas distinguish tumor subclasses with clinical implications. Proc Natl Acad Sci USA. 2001;98(19):10869–74.
7. Beck B, Blanpain C. Unravelling cancer stem cell potential. Nat Rev Cancer. 2013;13(10):727–38.

8. Zhang L, Chen W, Liu S, Chen C. Targeting Breast Cancer Stem Cells. Int J Biol Sci. 2023;19(2):552–70.
9. Bai X, Ni J, Beretov J, Graham P, Li Y. Cancer stem cell in breast cancer therapeutic resistance. Cancer Treat Rev. 2018;69:152–63.
10. Al-Hajj M, Wicha MS, Benito-Hernandez A, Morrison SJ, Clarke MF. Prospective identification of tumorigenic breast cancer cells. Proc Natl Acad Sci USA. 2003;100(7):3983–8.
11. Metzger E, Stepputtis SS, Strietz J, Preca BT, Urban S, Willmann D, et al. KDM4 Inhibition Targets Breast Cancer Stem-like Cells. Cancer Res. 2017;77(21):5900–12.
12. Li X, Strietz J, Bleilevens A, Stickeler E, Maurer J. Chemotherapeutic Stress Influences Epithelial-Mesenchymal Transition and Stemness in Cancer Stem Cells of Triple-Negative Breast Cancer. Int J Mol Sci. 2020;21(2).
13. Derakhshan F, Reis-Filho JS. Pathogenesis of Triple-Negative Breast Cancer. Annu Rev Pathol. 2022;17:181–204.
14. Su S, Chen J, Yao H, Liu J, Yu S, Lao L, et al. CD10(+)GPR77(+) Cancer-Associated Fibroblasts Promote Cancer Formation and Chemoresistance by Sustaining Cancer Stemness. Cell. 2018;172(4):841–e5616.
15. Han C, Liu T, Yin R. Biomarkers for cancer-associated fibroblasts. Biomark Res. 2020;8(1):64.
16. Chen X, Song E. Turning foes to friends: targeting cancer-associated fibroblasts. Nat Rev Drug Discovery. 2019;18(2):99–115.
17. Brogna MR, Varone V, DelSesto M, Ferrara G. The role of CAFs in therapeutic resistance in triple negative breast cancer: an emerging challenge. Front Mol Biosci. 2025;12:1568865.
18. Rafaeva M, Jensen ARD, Horton ER, Zornhagen KW, Strøbech JE, Fleischhauer L, et al. Fibroblast-derived matrix models desmoplastic properties and forms a prognostic signature in cancer progression. Front Immunol. 2023;14:1154528.
19. Muralidharan H, Hansen T, Steinle A, Schumacher D, Stickeler E, Maurer J. Breast Cancer Stem Cells Upregulate IRF6 in Stromal Fibroblasts to Induce Stromagenesis. Cells. 2024;13:17.
20. Su SA, Xie Y, Zhang Y, Xi Y, Cheng J, Xiang M. Essential roles of EphrinB2 in mammalian heart: from development to diseases. Cell communication signaling: CCS. 2019;17(1):29.
21. Su SA, Yang D, Wu Y, Xie Y, Zhu W, Cai Z, et al. EphrinB2 Regulates Cardiac Fibrosis Through Modulating the Interaction of Stat3 and TGF-β/Smad3 Signaling. Circul Res. 2017;121(6):617–27.
22. Piffko A, Uhl C, Vajkoczy P, Czabanka M, Broggini T. EphrinB2-EphB4 Signaling in Neurooncological Disease. Int J Mol Sci. 2022;23(3).
23. Yang D, Jin C, Ma H, Huang M, Shi GP, Wang J, et al. EphrinB2/EphB4 pathway in postnatal angiogenesis: a potential therapeutic target for ischemic cardiovascular disease. Angiogenesis. 2016;19(3):297–309.
24. Noren NK, Pasquale EB. Paradoxes of the EphB4 receptor in cancer. Cancer Res. 2007;67(9):3994–7.

25. Kakarla M, ChallaSivaKanaka S, Dufficy MF, Gil V, Filipovich Y, Vickman R et al. Ephrin B Activate Src Family Kinases in Fibroblasts Inducing Stromal Remodeling in Prostate Cancer. Cancers. 2022;14(9).
26. Strietz J, Stepputtis SS, Follo M, Bronsert P, Stickeler E, Maurer J. Human Primary Breast Cancer Stem Cells Are Characterized by Epithelial-Mesenchymal Plasticity. Int J Mol Sci. 2021;22(4).
27. Barbazan J, Pérez-González C, Gómez-González M, Dedenon M, Richon S, Latorre E, et al. Cancer-associated fibroblasts actively compress cancer cells and modulate mechanotransduction. Nat Commun. 2023;14(1):6966.
28. Egea J, Klein R. Bidirectional Eph–ephrin signaling during axon guidance. Trends Cell Biol. 2007;17(5):230–8.
29. Wilkinson DG. Multiple roles of eph receptors and ephrins in neural development. Nat Rev Neurosci. 2001;2(3):155–64.
30. Noren NK, Pasquale EB. Eph receptor–ephrin bidirectional signals that target Ras and Rho proteins. Cell Signal. 2004;16(6):655–66.
31. Zhang K, Guo L, Li X, Hu Y, Luo N. Cancer-associated fibroblasts promote doxorubicin resistance in triple-negative breast cancer through enhancing ZFP64 histone lactylation to regulate ferroptosis. J translational Med. 2025;23(1):247.
32. Veith I, Mencattini A, Picant V, Serra M, Leclerc M, Comes MC, et al. Apoptosis mapping in space and time of 3D tumor ecosystems reveals transmissibility of cytotoxic cancer death. PLoS Comput Biol. 2021;17(3):e1008870.
33. Duan W-L, Wang X-J, Gu L-H, Guo A, Ding Y-Y, Lin P, et al. NRG1/PDGFC loop between fibroblasts and cancer cells drives paclitaxel resistance via ferroptosis suppression in breast cancer. Cell Death Discovery. 2025;11(1):520.
34. Li X, Li Q, Yu X, Li H, Huang G. Reverse of microtubule-directed chemotherapeutic drugs resistance induced by cancer-associated fibroblasts in breast cancer. OncoTargets therapy. 2019;12:7963–73.
35. Begicevic RR, Falasca M. ABC Transporters in Cancer Stem Cells: Beyond Chemoresistance. Int J Mol Sci. 2017;18(11).
36. He J, Yu Y, He Y, He J, Ji G, Lu H. Chemotherapy induces breast cancer stem cell enrichment through repression of glutathione S-transferase Mu. Genes Dis. 2024;11(2):528–31.
37. Zheng Q, Zhang M, Zhou F, Zhang L, Meng X. The Breast Cancer Stem Cells Traits and Drug Resistance. Front Pharmacol. 2020;11:599965.
38. Soon PS, Kim E, Pon CK, Gill AJ, Moore K, Spillane AJ, et al. Breast cancer-associated fibroblasts induce epithelial-to-mesenchymal transition in breast cancer cells. Endocrine-related Cancer. 2013;20(1):1–12.
39. Maehira H, Miyake T, Iida H, Tokuda A, Mori H, Yasukawa D, et al. Vimentin Expression in Tumor Microenvironment Predicts Survival in Pancreatic Ductal Adenocarcinoma: Heterogeneity in Fibroblast Population. Ann Surg Oncol. 2019;26(13):4791–804.

40. Zhao Z, Li T, Yuan Y, Zhu Y. What is new in cancer-associated fibroblast biomarkers? Cell Communication Signal. 2023;21(1):96.
41. Richardson AM, Havel LS, Koyen AE, Konen JM, Shupe J, Wiles WG. Vimentin Is Required for Lung Adenocarcinoma Metastasis via Heterotypic Tumor Cell–Cancer-Associated Fibroblast Interactions during Collective Invasion. Clin Cancer Res. 2018;24(2):420–32.
42. Chen W, Jiang M, Zou X, Chen Z, Shen L, Hu J, et al. Fibroblast Activation Protein (FAP)+ cancer-associated fibroblasts induce macrophage M2-like polarization via the Fibronectin 1-Integrin α5β1 axis in breast cancer. Oncogene. 2025;44(28):2396–412.
43. Loh JJ, Ma S. Hallmarks of cancer stemness. Cell Stem Cell. 2024;31(5):617–39.
44. Albrengues J, Bertero T, Grasset E, Bonan S, Maiel M, Bourget I, et al. Epigenetic switch drives the conversion of fibroblasts into proinvasive cancer-associated fibroblasts. Nat Commun. 2015;6(1):10204.
45. Wang T, Fahrmann JF, Lee H, Li YJ, Tripathi SC, Yue C, et al. JAK/STAT3-Regulated Fatty Acid β-Oxidation Is Critical for Breast Cancer Stem Cell Self-Renewal and Chemoresistance. Cell Metabol. 2018;27(1):136–e505.
46. Cao C, Huang Y, Tang Q, Zhang C, Shi L, Zhao J, et al. Bidirectional juxtacrine ephrinB2/Ephs signaling promotes angiogenesis of ECs and maintains self-renewal of MSCs. Biomaterials. 2018;172:1–13.
47. Ramos Zapatero M, Tong A, Opzoomer JW, O'Sullivan R, Cardoso Rodriguez F, Sufi J, et al. Trellis tree-based analysis reveals stromal regulation of patient-derived organoid drug responses. Cell. 2023;186(25):5606–e1924.
48. Ding D, Wang X, Xuan R, Li R, Zhang Y, Wang Z. Ephrin–B2 promotes gastric cancer growth by inhibiting apoptosis and regulating the cell cycle via the Wnt/β–catenin signaling pathway. Int J Oncol. 2026;68(1).
49. Sasine JP, Kozlova NY, Valicente L, Dukov J, Tran DH, Himburg HA, et al. Inhibition of Ephrin B2 Reverse Signaling Abolishes Multiple Myeloma Pathogenesis. Cancer Res. 2024;84(6):919–34.
50. Zhang Q, Li J, Liu F, Hu J, Liu F, Zou J, et al. Ephrin B2 (EFNB2) potentially protects against intervertebral disc degeneration through inhibiting nucleus pulposus cell apoptosis. Arch Biochem Biophys. 2024;756:109990.
51. Wang HU, Chen Z-F, Anderson DJ. Molecular Distinction and Angiogenic Interaction between Embryonic Arteries and Veins Revealed by ephrin-B2 and Its Receptor Eph-B4. Cell. 1998;93(5):741–53.
52. Adams RH, Diella F, Hennig S, Helmbacher F, Deutsch U, Klein R. The Cytoplasmic Domain of the Ligand EphrinB2 Is Required for Vascular Morphogenesis but Not Cranial Neural Crest Migration. Cell. 2001;104(1):57–69.

Figures

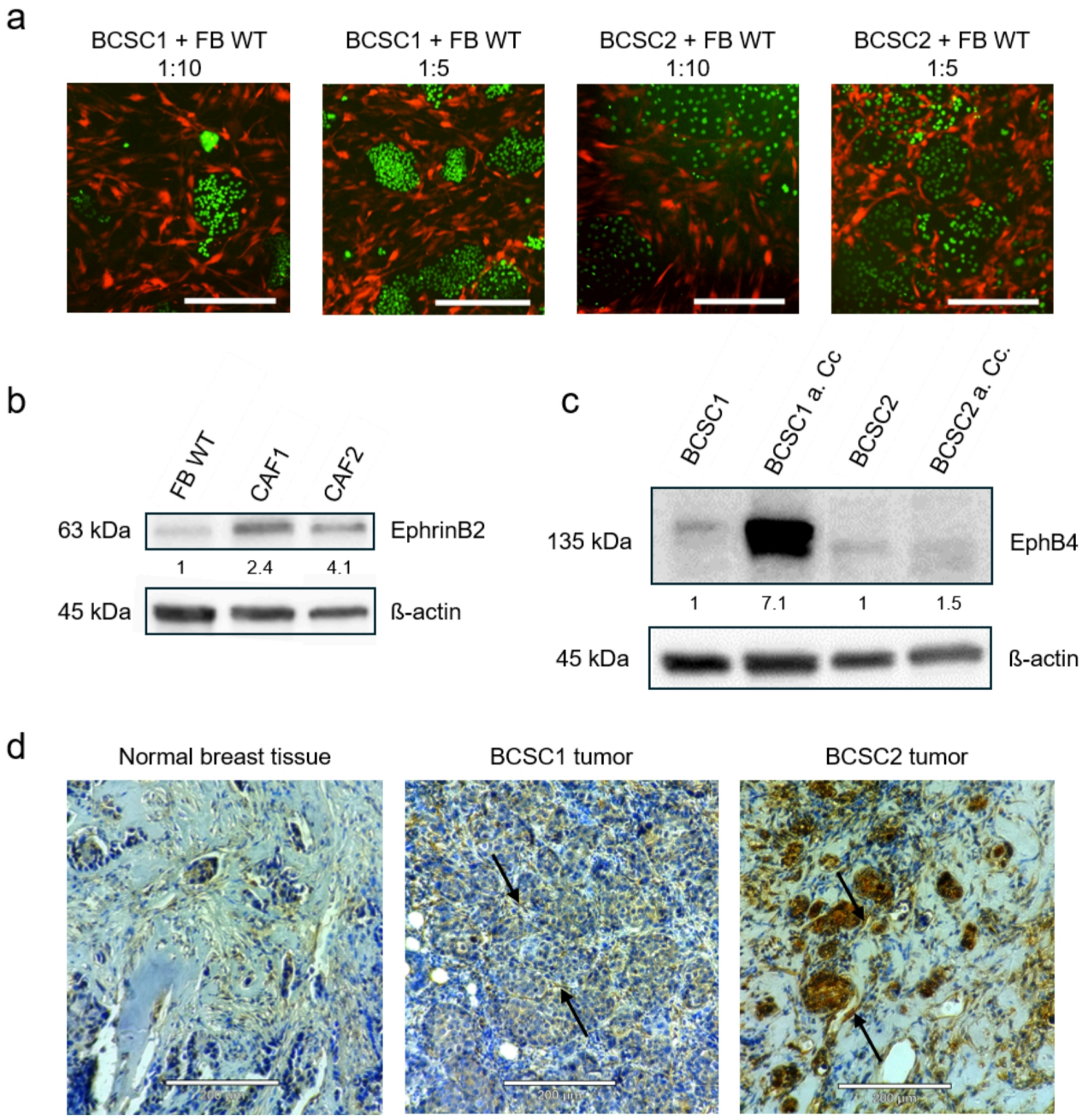


Figure 2

EphrinB2 is upregulated in CAFS in breast cancer

a) Cocultures of BCSC1 (GFP) or BCSC2 (GFP) with fibroblasts (FB WT, mCherry) in a ratio of 1:10 and 1:5, 10x magnification with IncuCyte®. Scalebar represents 400 µm **b)** Western blot and quantification of EphrinB2 in fibroblasts before (FB WT) and after coculture and FACS sort with BCSC1 (CAF1) and BCSC2 (CAF2) n=3, mean **c)** Western blot and quantification of EphB4 in BCSCs before and after coculture (a. Cc) and FACS sort with FB WT n=3, mean d) Staining of EphrinB2 in normal breast tissue (left), murine

tumor with BCSC1 and fibroblasts (middle) and murine tumor with BCSC2 and fibroblasts (right). Black arrows indicate EphrinB2-expressing CAFs.

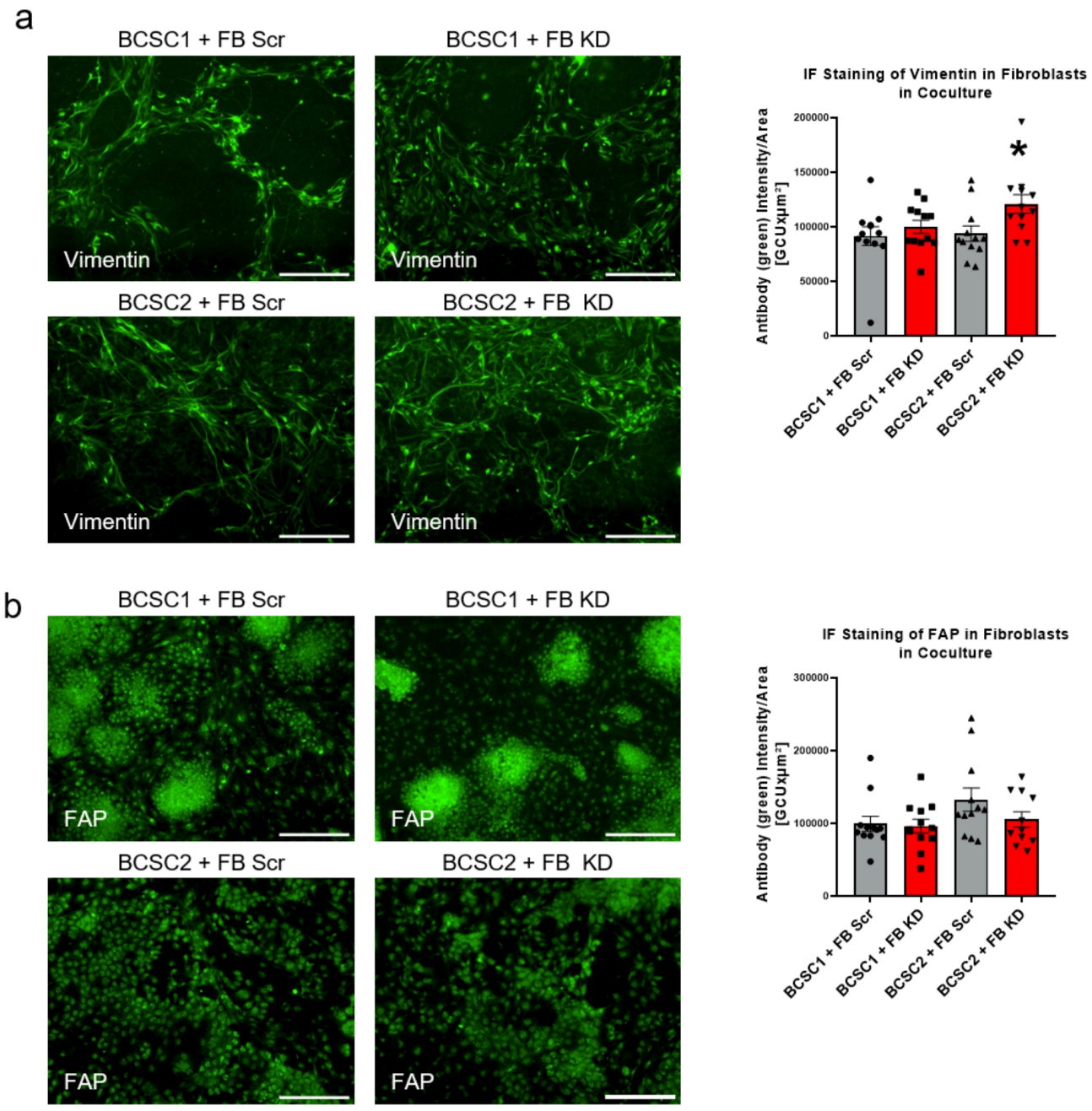


Figure 4

EphrinB2 knockdown in fibroblasts increases Vimentin and decreases FAP expression

a) Representative images and quantification of Vimentin staining in cocultures of BCSC1 or BCSC2 with knockdown or scramble fibroblasts in a ratio of 1:2, 20x magnification, imaging and analysis with IncuCyte® n=3 mean ± SEM BCSC2: p=0.0222. Scalebar represents 200µm **b)** Representative images

and quantification of FAP staining in cocultures of BCSC1 or BCSC2 with knockdown or scramble fibroblasts in a ratio of 1:2, 20x magnification, imaging and analysis with IncuCyte® n=3 mean ± SEM. Scalebar represents 200µm. . (*) is defined as p<0.05; (**) is defined as p<0.01; (***) is defined as p<0.001; (****) is defined as p<0.0001.

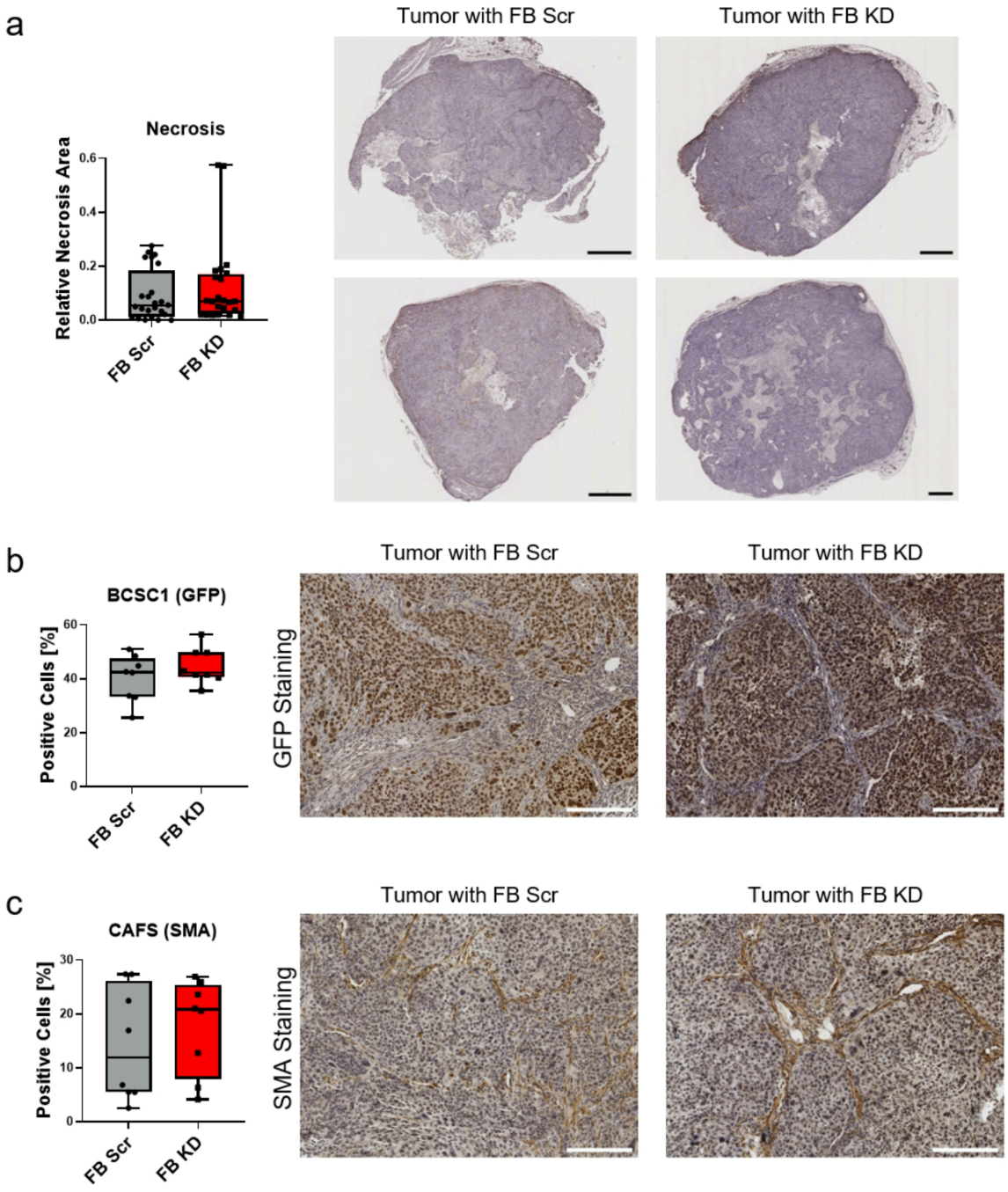


Figure 7

Tumors with knockdown-fibroblasts consist of a higher amount of BCSCs and CAFs

a) Representative images and quantification of necrosis area relative to tumor area, three images per tumor were analyzed, eight tumors per group. Scale bar represents 1mm **b)** Representative images and quantification of immunohistochemistry staining of GFP, so of the BCSCs in murine tumors consisting of BCSC1 and FB Scr or FB KD n=8 Scalebar represents 200µm **c)** Representative images and quantification of immunohistochemistry staining of SMA, so of the CAFs in murine tumors consisting of BCSC1 and FB Scr or FB KD n=8. Scalebar represents 200µm

Supplementary Files

This is a list of supplementary files associated with this preprint. Click to download.

- SupplementaryFiguresBCR.pdf